



An airborne study of the aerosol effect on the dispersion of cloud droplets in a drizzling marine stratocumulus cloud over eastern China

Fei Wang^a, Zhanqing Li^{b,*}, Delong Zhao^c, Xincheng Ma^c, Yang Gao^a, Jiujiang Sheng^c, Ping Tian^c, Maureen Cribb^b

^a Key Laboratory for Cloud Physics, Chinese Academy of Meteorological Sciences, Beijing 100081, China

^b Department of Atmospheric and Oceanic Science, University of Maryland, College Park, MD 20742, USA

^c Beijing Weather Modification Office, Beijing 100081, China

ARTICLE INFO

Keywords:

Stratocumulus
Aerosol-cloud interactions
Relative dispersion
Indirect effect

ABSTRACT

Detailed airborne measurements were carried out to explore aerosol-cloud interactions and cloud microphysical properties in a drizzling marine stratocumulus cloud deck over eastern China. Results show that the collision-coalescence of cloud droplets, the condensation of small droplets, and the collision-induced break-up of drizzle were the dominant microphysical processes in the sampled water cloud parcel. The region in the vicinity of the cloud's lateral boundary was spatially divided into sub-regions to better understand aerosol and droplet interactions. Relationships between the relative dispersion (ϵ) and the cloud's microphysical and dynamical characteristics were also examined. A negative relation was found between ϵ and the cloud droplet number concentration, with ϵ showing a close relationship with the liquid water content (LWC) and updraft velocity. When LWC was greater than $\sim 0.75 \text{ g kg}^{-1}$, the range of ϵ values narrowed, and updrafts dominated. By introducing ϵ in the cloud droplet effect radius (R_e) parameterization, we find that ϵ can further affect indirect forcing by changing the R_e distribution for the cloud examined in this study. The dispersion effect (DE) was estimated using the effective radius ratio and the specific cloud water content. An in-depth analysis indicates that DE may offset the Twomey effect by $\sim 12\%$. Two different methods of estimating the indirect effect (IE) yielded close values (0.084 and 0.077), suggesting that introducing DE into the estimation had a small influence on the IE calculation in the drizzling marine stratocumulus cloud of this study. Note that the estimated IE has a large uncertainty, given the large biases in the cloud properties measured.

1. Introduction

As important parts of the earth's atmosphere, clouds cover more than 67% of the globe (King et al., 2013). The dominant cloud type is stratocumulus, covering approximately 20% of the Earth's water and land surfaces. Stratocumulus clouds are more expansive than any other cloud type, making them extremely important for maintaining the energy balance and the moisture budget of the earth (Wood, 2012). Radiative cooling, precipitation formation, and aerosol-cloud interactions are the primary mechanisms for maintaining and regulating feedbacks of stratocumulus clouds.

Stratocumulus clouds are sensitive to ambient aerosol perturbations, leading to possible significant changes in cloud macroscopic and microscopic characteristics (Li et al., 2019). Well known is that an increase in aerosol loading results in an increase in the number of cloud

droplets and a decrease in cloud droplet size, enhancing the cloud albedo (first indirect effect, or IE) and reducing the drizzle formation efficiency (second IE) for a fixed cloud water content (Albrecht, 1989; Twomey, 1974). However, many in situ and remote sensing studies have found distinct, even opposite, observational evidence of the above hypothesis (Grandey and Stier, 2010; Qiu et al., 2017; Yuan et al., 2008). Aerosol-cloud interactions (ACI), as well as aerosol-radiation interactions, are complex ways by which aerosols affect Earth's weather and climate (Li et al., 2016, 2017, 2019; Zhao et al., 2020). In the search for ways to study the complicated relationship between aerosol particles and cloud droplets, relative dispersion (ϵ , defined as the ratio of the cloud droplet spectral width to the cloud droplet mean radius) and its influence on the IE (defined as the dispersion effect) have been examined (Liu and Daum, 2002). Recent studies have shown that dispersion plays an important role in cloud parameterization schemes in general

* Corresponding author.

E-mail address: zli@atmos.umd.edu (Z. Li).

<https://doi.org/10.1016/j.atmosres.2021.105885>

Received 5 May 2021; Received in revised form 11 October 2021; Accepted 12 October 2021

Available online 14 October 2021

0169-8095/© 2021 Published by Elsevier B.V.

circulation models (GCMs) through its effects on cloud albedo, the cloud droplet number concentration (N_c) and size distribution, water content, drizzle formation, raindrop sedimentation, entrainment, and mixing processes, among others (Anil Kumar et al., 2016; Ansari et al., 2020; Liu et al., 2006a, 2006c; Lu et al., 2020; Pandithurai et al., 2012; Pardo, 2021; Tas et al., 2012; Wang et al., 2011; Xie and Liu, 2013). The ε of cloud droplets has been a focus in cloud physics over the last two decades (Desai et al., 2019).

Based on conclusions supported by numerical modeling, observational data, and theoretical studies, research on ε has mainly focused on four things: (1) the relationship between ε and droplet (or background aerosol) concentration, (2) the correlation between ε and cloud microphysics or dynamics (e.g., turbulence, updrafts, collision-coalescence, raindrop sedimentation, meteorological conditions, entrainment, and the mixing process), (3) the effect of ε on the autoconversion process (influence on the second IE), and (4) indirect warming by the dispersion effect (influence on the first IE). Previous studies indicate that there is a direct dependence of ε on N_c . An increase in ε with N_c was predicted by condensation theory (Liu et al., 2006c; Yum and Hudson, 2005), and similar positive correlations were also obtained in observational studies (Anil Kumar et al., 2016; Liu and Daum, 2002; Martin et al., 1994; Pandithurai et al., 2012; Prabha et al., 2012; Wang et al., 2021). However, some recent studies derived a negative ε - N_c relationship (Cecchini et al., 2017; Desai et al., 2019; Lu et al., 2012a; Lu et al., 2007; Ma et al., 2010; Pawlowska et al., 2006) or an ambiguous ε - N_c relationship (Brenquier et al., 2011; Deng et al., 2009; Lu et al., 2008; Tas et al., 2015; Zhao et al., 2006) from in situ measurements. Many laboratory studies also concluded that ε decreases with increasing N_c in most cloud chamber experiments (Chandrakar et al., 2016, 2018; Desai et al., 2018). This suggests that the variation in cloud droplet ε is complex, sensitive to many factors, such as aerosol loading, aerosol chemical composition, vertical velocity (w), collision-coalescence, entrainment, and mixing (Lu et al., 2012a; Martins and Silva Dias, 2009; Wang et al., 2011; Yum and Hudson, 2005). The ε value also varies considerably in different cloud parcels (Arabas et al., 2009; Pawlowska et al., 2006; Prabha et al., 2012) or at different evolutionary stages of cloud development (Tas et al., 2012, 2015), likely due to the dominant effects of pollutant loading or updrafts in cloud.

An ε - N_c correlation or a β - N_c correlation, where β is the effective radius ratio (a function of ε), has been employed to evaluate the IE in ACI studies (Liu and Daum, 2002; Pandithurai et al., 2012; Rotstajn and Liu, 2003; Xie and Liu, 2013; Xie et al., 2017). Ghan et al. (2001) indicated that about half of the indirect radiative forcing is due to droplet size variation. According to Liu and Daum (2002), (1) a positive ε - N_c relationship significantly overestimated IE , and (2) IE could be reduced by 10–80%, depending on the parameterization of ε . By introducing the dispersion effect in a GCM using a linear relationship between β and N_c , the global mean IE estimation was reduced by ~15% (Peng and Lohmann, 2003). Furthermore, an increased ε may increase the effective radius and autoconversion efficiency, influencing the second aerosol IE . Xie and Liu (2009, 2011) found a positive correlation between ε and the cloud water autoconversion efficiency. If ε is large, the well-mixed small and large droplets would enhance the collision-coalescence process, promoting warm-rain initiation. Numerical modeling studies have shown that ε (including the ε - N_c relationship) affects cloud microphysical properties and surface precipitation substantially under both clean and polluted background conditions (Xie et al., 2013).

Owing to the diversity and complexity of ACI studies, more work needs to be done to understand the underlying mechanisms. As a key factor in the study of ACI, our understanding of ε and its effects is incomplete. To better understand and parameterize ε , more theoretical, observational, and numerical studies are urgently needed (Lu et al., 2020).

Taking advantage of some comprehensive air-borne observational data required to examine the aerosol-cloud relationship in drizzling marine stratocumulus clouds, this study emphasizes the interaction

between aerosols and cloud droplets and the effects of ε on the parameterization of R_c and the estimation of IE . Revealing ε and its effects can help reduce the uncertainty and the discrepancy between climate model estimates and satellite observations (Xie et al., 2017). Results obtained here may promote studies on ACI, which in turn affects aerosol IE evaluations. Section 2 describes the geographical location of interest, the instruments used, the flight strategy implemented, and meteorological conditions. Section 3 presents intra-cloud aerosol and cloud droplet microphysical properties. Also presented is the calculation of ε and other related factors, such as updraft velocity and water mixing ratio, at different altitudes to discuss plausible physical mechanisms. Finally, with the dispersion effect taken into account, R_c is parameterized, and IE is evaluated. Major concluding remarks are given in Section 4.

2. Data and experiment

2.1. Flight and leg details

To better understand ACI and the role of aerosols in cloud microphysics, in situ aircraft measurements were conducted off the coastal region of eastern China on 4 September 2016. Two turboprop aircrafts (Y-12 and Modern Ark 60) were deployed to measure aerosol and cloud microphysical properties in marine stratocumulus clouds. The Modern Ark 60 also carried out a mission of cloud seeding by introducing hygroscopic particles into a convective cell (Wang et al., 2019). The instrumented Y-12 aircraft carried out intensive cloud and aerosol observations, which is the primary objective of this study. Fig. 1a shows the surrounding terrain and flight trajectory of the Y-12. The aircraft took off from Quzhou Airport (28.97°N, 118.9°E), climbed to ~3500 m, and flew in the northeasterly direction for ~250 km, reaching the coastal area of interest for the experiment. The aircraft descended into the middle of a cloud parcel then ascended to perform cloud sampling in step levels of ~300 m (from ~2550 m to ~3150 m, Fig. 1b). The sampled cloud was ~30 km northwest of the Modern Ark 60 cloud-seeding region, and the initiation of cloud measurements was ~3 h after seeding ended. Since the wind direction was northeasterly at the seeding altitude [as seen in Fig. 2 here and supplemental Fig. S1 in Wang et al., 2019], the sampled cloud in this study was confirmed not polluted by seeding agents. Fig. 1b shows the three-dimensional flight path and liquid water content (LWC) along the flight path during cloud penetration.

High-resolution aircraft measurements of ambient aerosol and droplets in clouds give detailed information about the aerosol-cloud interaction process. During cloud penetration, the strategy of making intra-cloud aircraft measurements was to sample aerosols and cloud droplets at an almost constant level in the lateral cloud boundary. The Y-12 descended to do cloud profiling at three levels covering the middle and upper parts of the cloud. The aircraft maintained a straight, level path to measure updrafts and downdrafts when sampling at the three cloud levels. A spiral flight pattern from ~3150 m to ~4400 m (corresponding to the cloud-top height) was also performed before the aircraft turned back to base.

Fig. 1c shows the visible image taken at 06:30 UTC on 4 September 2016 from the Gaofen 4 geostationary satellite. The diffuse grayish-white clouds are the upper-layer continental cloud deck, and the denser, bright clouds are lower-layer clouds, i.e., exterior cloud bands from Typhoon Namtheun (2016). The dual-layer cloud structure over the experimental region was also confirmed by satellite-retrieved cloud-top heights (from Himawari-8) and sounding data [Fig. 1 and S1 in (Wang et al., 2019)]. The lower-layer cloud with a higher cloud water content contributed the most to the cloud optical thickness. The presence of this two-layer cloud field led to the accumulation of unstable energy over this coastal region (K-index was ~30). The marine stratocumulus clouds were producing substantial drizzle and raindrops, documented by airborne probes and ground-based radar.

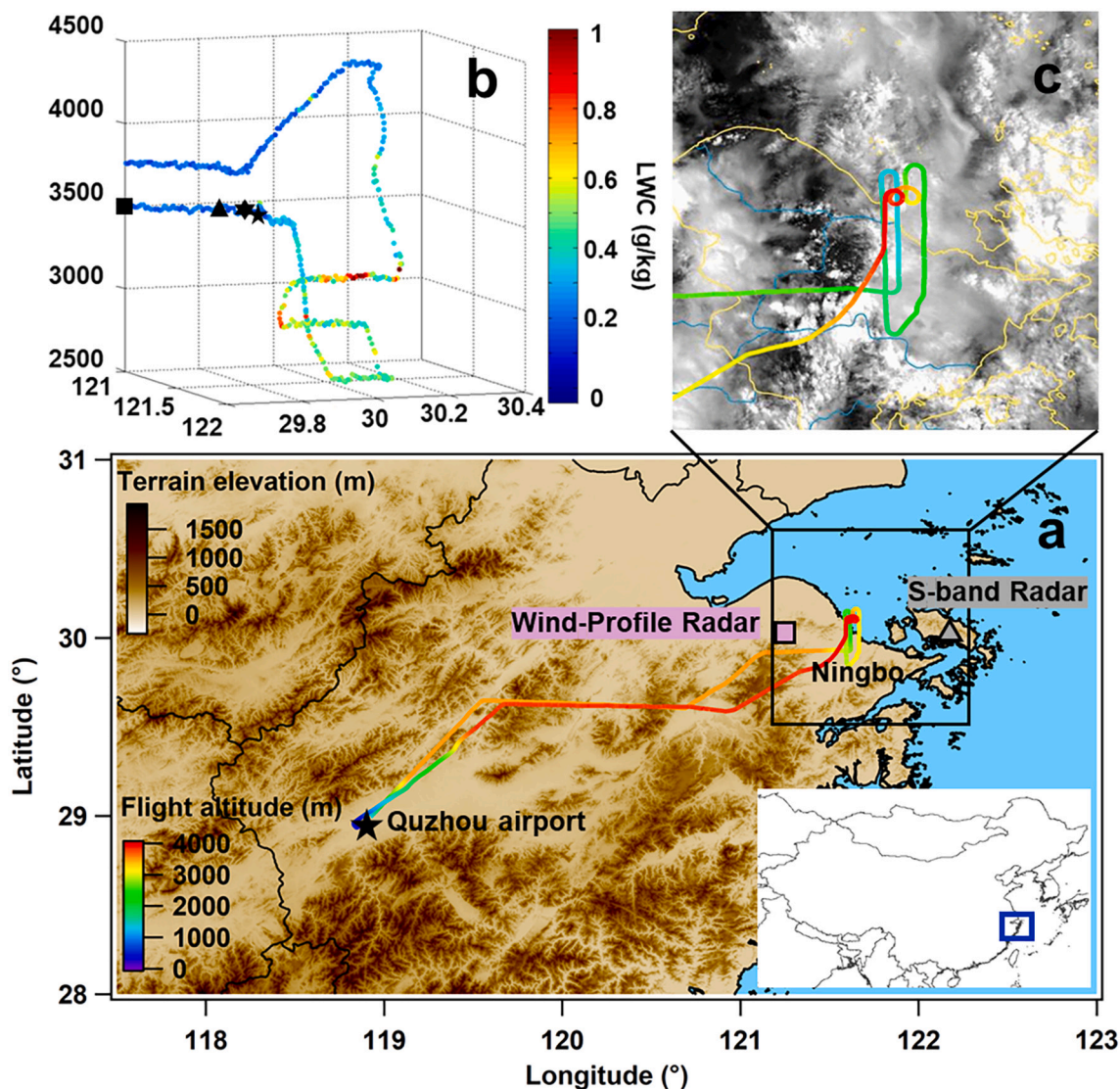


Fig. 1. Y-12 flight track during the study. (a) Geographical location of the experimental region, (b) three-dimensional routes, colored by the liquid water content (LWC), and (c) the visible image from the geostationary Gaofen 4 satellite at 06:30 UTC on 4 September 2016, showing the dual-layer cloud structure over the experimental region. Panels (b) and (c) show the flight track between 06:20 and 07:30 UTC when the aircraft conducted a specific pattern of cloud profiling over the Ningbo region. The pattern started with a profile ascending from an altitude of ~ 2550 m to ~ 3150 m (in step levels of ~ 300 m), then continued ascending to the cloud-top height (~ 4400 m) before turning back to base. The black symbols in (b) are described in Fig. 6.

2.2. Data and instrumentation

Measurements of ambient aerosols and droplets within the cloud were obtained using aircraft-mounted probes from Droplet Measurement Technology (DMT, USA), including a Passive Cavity Aerosol Spectrometer Probe (PCASP) for measuring aerosol particle sizes ranging from 0.1 to 3 μm , a Cloud and Aerosol Spectrometer (CAS), a Cloud Imaging Probe (CIP), a Precipitation Imaging Probe (PIP) measuring the cloud droplet size distribution from 0.6 to 6200 μm , a Hotwire sensor measuring the LWC (also expressed as q_{Hotwire}), and an Airborne Integrated Meteorological Measurement System (AIMMS-20) probe measuring temperature (T), relative humidity (RH), and w . All instruments were calibrated in the laboratory before the field campaign. Counts from the first two bins of the CIP and PIP probes were excluded since the sample volume for the droplets was difficult to determine. Here, the CAS-measured cloud droplet diameters ranged from 3 to 50 μm , the CIP-measured drizzle droplets ranged from 62.5 to 1000 μm , and the CIP-measured raindrops were greater than 1000 μm . The uncertainties of the DMT probes and the CAS- or CIP-derived droplet LWC

have been described in previous studies (Baumgardner et al., 2001; Kleinman et al., 2012; Lance, 2012). Due to the baseline drift, the zero offset of the Hotwire probe was corrected by recording the specific time of entering the cloud and after that, calculating a 2-min running average of LWC. Hotwire-measured LWCs agreed well with CAS-estimated LWCs (correlation coefficient equal to ~ 0.93 , figure not shown).

Aerosol information is typically obtained from below cloud bases in most ACI studies. Information about ambient aerosols used in this study were derived from PCASP measurements made at the lateral boundary before cloud penetration. Since the size range (0.1–3 μm) covers mainly accumulation-mode aerosols, the aerosol concentration in this size range is referred to as the pre-cloud aerosol concentration (N_{acc}). Cloud temperatures were restricted to above 0 $^{\circ}\text{C}$ to ensure that the cloud was in the liquid phase. The typical flight speed was 60–70 m s^{-1} , and the data acquisition time was 1 Hz in this study.

Fig. 1a shows the locations of the Doppler radar and the wind profile radar. The ground-based S-band Doppler radar (marked as a gray triangle in Fig. 1a), located in Zhoushan (30.07 $^{\circ}\text{N}$, 122.11 $^{\circ}\text{E}$, ~ 438 m above sea level), provided information about drizzle and raindrops. The

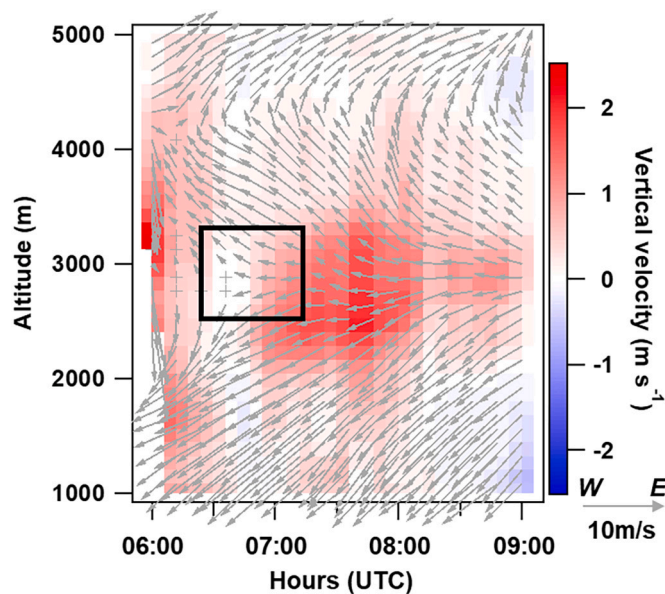


Fig. 2. Horizontal (gray arrows) and vertical (colour-shaded area) wind measured by the wind profile radar from 06:00 to 09:00 UTC on 4 September 2016. The black rectangle indicates the approximate spatial and temporal scales of the case-study cloud.

volume scan pattern is the standard mode for observing precipitation at 6-min intervals, with a minimum elevation angle of $\sim 0.5^\circ$. The wind profile radar (30.17°N , 121.25°E , marked as a pink square in Fig. 1a), deployed northwest of Ningbo, monitored the temporal evolution of wind profiles at a temporal resolution of 6 min.

3. Results and discussion

3.1. Intra-cloud microphysical properties

Three criteria were used in this study to determine if a record was water cloudy [Terai et al., 2014; Zhang et al., 2011; Zhao et al., 2019]: (1) cloud droplet number concentration $\geq 10 \text{ g cm}^{-3}$ (as measured by the CAS probe), (2) cloud water mixing ratio $\geq 0.01 \text{ g kg}^{-1}$ (from either the Hotwire probe or the CAS calculation), and (3) ambient $T \geq 0^\circ\text{C}$ (as measured by the AIMMS-20). Every group of five consecutive records, shifting by one record forward each time, was examined. Any group with less than five records satisfying the criteria was excluded. In this way, non-cloudy regions were identified.

Fig. 3 shows aerosol and cloud microphysical parameters during the ~ 30 -min period when the Y-12 aircraft flew through the cloud. Also shown are radar reflectivity, T , RH , and LWC along the flight track. The ambient N_{acc} was $\sim 42.4 \pm 13.6 \text{ cm}^{-3}$ at the flight altitude. The maximum and mean N_c measured by the CAS was 288.5 cm^{-3} and $47.0 \pm 33.9 \text{ cm}^{-3}$, respectively. The average R_e was $12.8 \pm 2.8 \mu\text{m}$. Table 1 gives detailed information about the microphysical parameters measured. The observed large droplets indicate that precipitation was already initiated (Rosenfeld and Gutman, 1994; Rosenfeld and Lensky, 1998). Maximum and mean reflectivity was $\sim 30.3 \text{ dBz}$ and $\sim 12.7 \text{ dBz}$, respectively, suggesting the inhomogeneity of precipitation particles in the cloud.

Previous studies (Tas et al., 2012, 2015; Terai et al., 2014) have suggested that microphysical parameters change constantly in different parts of a cloud or at different stages of cloud development. It is generally accepted that N_c changes little with altitude under an adiabatic condition, although large values of N_c might appear in the middle or upper part of a cloud during cloud swelling (Pawlowska et al., 2006). Fig. 4 shows the number concentration, effective radius, and spectra of cloud droplets (top panels) and drizzle drops (bottom panels) measured

at each horizontal flight leg penetrating the cloud. The altitudes of the horizontal traverses were $\sim 2550 \text{ m}$ (level I), $\sim 2850 \text{ m}$ (level II), and $\sim 3150 \text{ m}$ (level III), lasting 6–7 min at each level. Both N_c and the cloud droplet effective radius ($R_{e,c}$) increased with altitude. Cloud droplets grew from levels I to III, with a narrower spectrum at level I than at level III (Fig. 4c). Based on the vertical distribution of drizzle drops (i.e., number concentration (N_d) decreasing and effective radius ($R_{e,d}$) increasing with altitude), a large number of cloud droplets collided then coalesced with falling drizzle drops, lowering N_c at level I. At the same time, some of the drizzle drops broke into small droplets through collision during their rapid downward motion. According to Pruppacher and Klett (2012), droplets smaller than 4.5 mm are not prone to breaking up under stable conditions. However, PIP-measured droplets bigger than 4 mm were rarely seen during cloud sampling, so compared to self-break-up, the collision-induced break-up mechanism was considered to be dominant in this cloud. As a result, updrafts promoted the collision and coalescence of small droplets (likely produced by the collisional break-up of drizzle drops), resulting in drizzle sizes increasing with altitude (corresponding to the larger $R_{e,d}$ at level III). This was confirmed by CIP-generated 2D images and Hotwire-measured LWC at the three levels (Fig. 5). Although there were plenty of drizzle drops and cloud droplets at level III (gray dots in Fig. 5d), the coalescence of cloud droplets and the break-up of drizzle drops made N_c decrease and $N_d (< 400 \mu\text{m})$ increase during drop falling. In particular, a number of small cloud droplets ($R_{e,c}$ of $\sim 5 \mu\text{m}$) were seen at level III (Fig. 4b). From the higher LWC (calculated by the CAS) and the appearance of small droplets at this level, the condensation of small droplets may have also benefitted the formation of drizzle drops in the case-study cloud. Furthermore, the enhancement of turbulence (as seen in Fig. 5c, where the updraft velocity and its variability were maximal at level III) promoted collision-coalescence of droplets at that level. This process has a significant impact on the emergence of drizzle drops and precipitation formation. Chen et al. (2018a, 2018b) made the same inference by a modeling study.

3.2. Aerosol and cloud microphysics during cloud penetration

To study the aerosol IE, aerosol and cloud microphysical characteristics near the cloud lateral boundary were analyzed. Most previous studies have focused on the interactions between aerosols, cloud condensation nuclei, and cloud droplets at the bottom of cumulus clouds to study the activation process of aerosols to cloud drops. However, aircraft data from the cloud lateral-boundary region are valuable for studying entrainment, although nucleation may also take place. Entrainment processes at the cloud top or lateral boundary are all important during cloud development (Burnet and Brenguier, 2007; Grabowski and Pawlowska, 1993; Lu et al., 2012b; Stommel, 1947; Tölle and Krueger, 2014). During cloud expansion, ambient air masses are entrained into the cloud through the lateral boundary, progressively diluting the cloud (De Rooy et al., 2013). Here, since part of the cloud reached the ground through drizzling (or raining), and w at the cloud base was relatively weak, the sampled cloud was considered a non-cumulus cloud system in the traditional sense and in the decaying to mature stage of its lifecycle. As such, the aerosol effect on cloud nucleation was much smaller than that in a developing (or non-precipitating) stratocumulus. This section thus aims to study ACI by analyzing aircraft data in the vicinity of the cloud lateral boundary.

Fig. 6 shows the data collected during the first cloud penetration as a function of distance from the cloud. The aircraft experienced a complex process from the cloud-free area to the interior of the cloud. Taking the variations of aerosol, cloud and meteorological parameters into account, four zones are defined: distant from the cloud, a transition zone near the cloud, at the cloud boundary, and inside the cloud. Distant from the cloud, both ambient RH and N_{acc} were low and generally nearly constant at the same altitude. Nearing the cloud, the ambient RH gradually increased to $\sim 80\%$. The fluctuating value was probably due to the

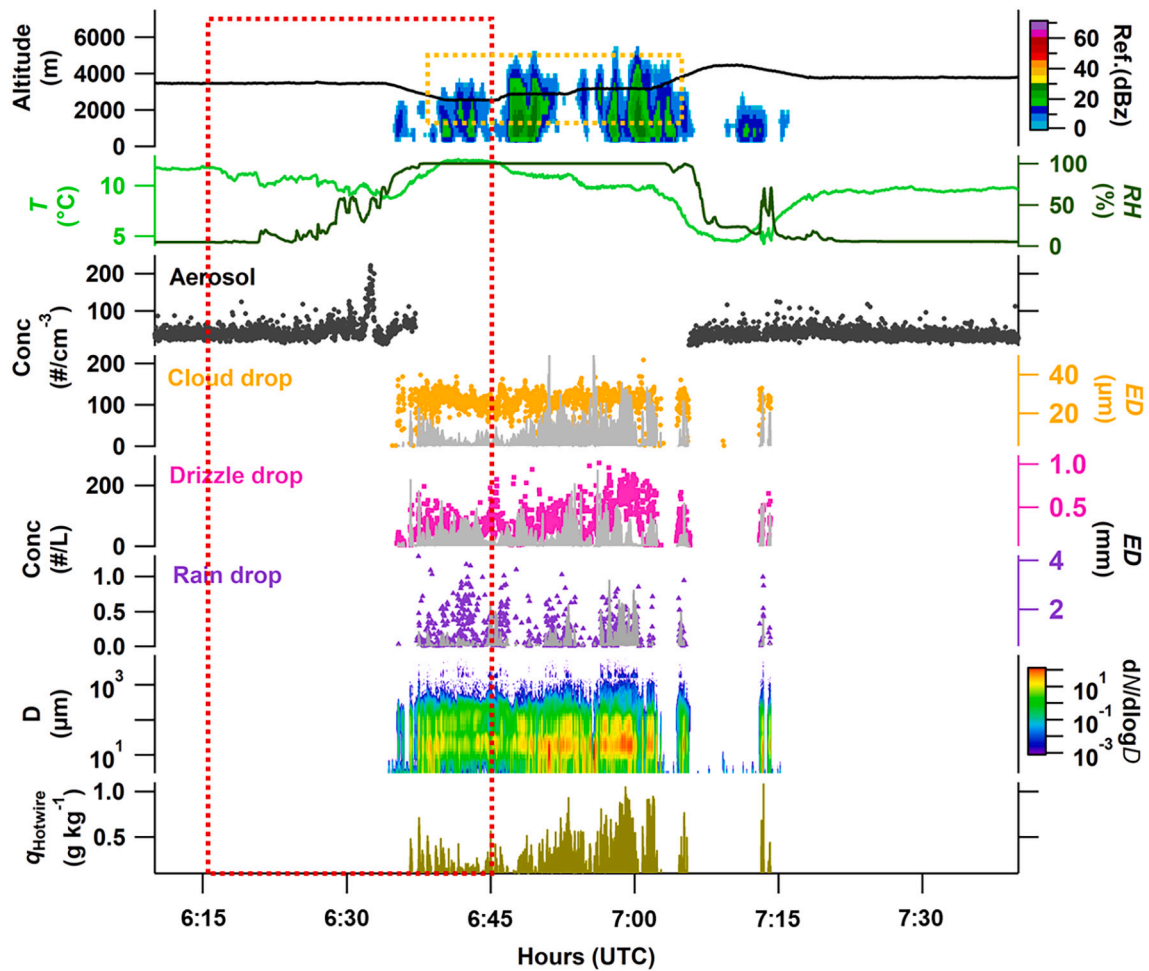


Fig. 3. Time series of (from top to bottom) radar reflectivity along the flight track, temperature (T) and relative humidity (RH), aerosol concentration, cloud droplet size (effective diameter, ED) and concentration (Conc.), drizzle drop size and concentration, raindrop size and concentration, spectrum of droplets in the cloud, and mixing ratio ($q_{Hotwire}$) in the case-study cloud. The yellow dashed box in the topmost time series shows when cloud sampling at three altitudes occurred. The red dashed box outlines the period of 06:15–06:45 UTC, the focus for further discussion in Fig. 6. (For interpretation of the references to colour in this figure legend, the reader is referred to the web version of this article.)

Table 1

Statistics describing the ambient aerosol and microphysical parameters of the case-study cloud.

Variable	Formula	Maximum	Mean
N_{acc} (cm^{-3})	$N = \sum n_i$	222.7	42.4 ± 13.6
N_c (cm^{-3})		288.5	47.0 ± 33.9
N_d (L^{-1})		249.9	38.9 ± 35.3
$R_{e,acc}$ (μm)	$R_e = \sum n_i r_i^3 / \sum n_i r_i^2$	2.67	0.24 ± 0.21
$R_{e,c}$ (μm)		18.51	12.80 ± 2.81
$R_{e,d}$ (μm)		978.9	348.7 ± 186.2
q_c ($g\ kg^{-1}$)		1.45	0.30 ± 0.27
q_d ($g\ kg^{-1}$)	$q = \frac{4}{3} \pi \rho (\sum n_i r_i^3)$	1.33	0.17 ± 0.16
$q_{Hotwire}$ ($g\ kg^{-1}$)		1.05	0.25 ± 0.21

[(n_i indicates the aerosol, cloud droplet, or drizzle droplet observed in the i th bin of the PCASP, CAS, or CIP; r_i is the mean radius in the i th bin; ρ is the density of liquid water (here, $\rho = 1.0\ g\ cm^{-3}$)].

inhomogeneous distribution of the cloud outer boundary. Meanwhile, aircraft-measured w fluctuated more significantly inside the cloud than outside, suggesting that turbulence and the entrainment process were strengthening in this zone. N_{acc} slightly increased, accompanied by peak values corresponding to low values of RH . The maximum N_{acc} was about 5 to 8 times than that of N_{acc} distant from the cloud, with the aerosol size changing little. This was probably due to the entrainment and mixing of

dry air, with evaporation of cloud droplets causing an increase in N_{acc} . Note that the size of the evaporated cloud droplets was approximately equivalent to the ambient accumulation-mode aerosol size. Furthermore, the evaporation of cloud droplets may also cause N_c to decrease and ambient N_{acc} to increase (Kleinman et al., 2012). At the cloud boundary, the measured air parcel was nearly saturated. N_{acc} was lower than that in the transition zone near the cloud but somewhat higher than that further away from the cloud. The CAS captured cloud droplets $>3\ \mu m$. Hygroscopic growth and entrainment of accumulation-mode aerosols in a moist environment may explain the patchy distribution of cloud droplets (from a few microns to tens of microns). The RH reached and exceeded 100% inside the cloud, and the cloud and drizzle drop concentrations increased rapidly. As the aircraft flew deeper into the cloud, the cloud water mixing ratio measured by the Hotwire probe ($q_{Hotwire}$) gradually increased, and w varied more.

Changes in the background environment of the atmosphere may alter aerosol physical or chemical characteristics due to the hygroscopic effect and nucleation, leading to a variation in aerosol size distribution. The aerosol spectrum is an important indicator describing the aerosol size distribution and determining its life cycle in the atmosphere. As seen in Fig. 6, PCASP-measured aerosol numbers and sizes show significant discrepancies in the different zones. Fig. 7 shows mean aerosol spectrum distributions distant from the cloud, near the cloud, and at the cloud boundary. Being away from the cloud, N_{acc} decreased exponentially

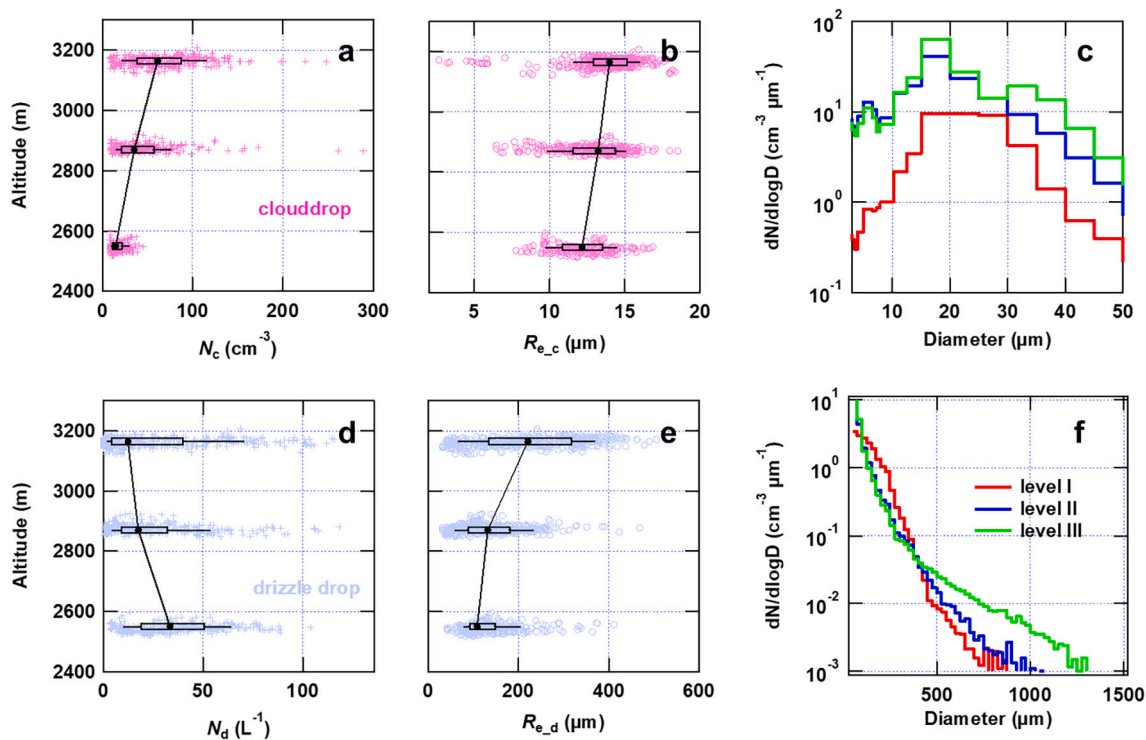


Fig. 4. Vertical variations of (a) the cloud droplet number concentration, (b) the cloud droplet effective radius, (d) the drizzle drop number concentration, and (e) the drizzle drop effective radius at the three levels sampled (level I: ~ 2550 m, level II: ~ 2850 m, level III: ~ 3150 m). The boxes and whiskers represent the horizontal mean (solid circles), 25th and 75th percentiles (boxes), and 10th and 90th percentiles (left and right whiskers) of the data. Also shown are the mean (c) cloud droplet and (f) drizzle drop spectra at the three levels.

with increasing aerosol size, with the diameter of accumulation-mode aerosols reaching ~ 0.5 μm . As the aircraft approached the cloud, N_{acc} significantly increased, and the spectrum width broadened. Aerosol particle sizes fell mostly in the range of 0.1 μm to 0.3 μm . The exchange of substances between the cloud and the ambient atmosphere via entrainment, mixing, and evaporation resulted in an increase in aerosol number concentration in this zone. The N_{acc} at the cloud boundary was lower than that in zones further away from the cloud. The spectrum widened significantly, and the mean diameter of particles increased by approximately an order of magnitude. Several reasons may explain why large particles (>1 μm) were captured in this zone. The most likely explanation is the hygroscopic growth of aerosol particles caused by the moist environment. Another possible reason is that cloud droplets may have been mixed in with aerosol particles in the PCASP inlet.

Since the aerosol size distribution can be approximately characterized as a continuous spectrum, a distribution function can describe it. Lognormal, power exponential, and gamma functions are common functions expressing the aerosol spectrum distribution. In this study, a multiple-lognormal function was superimposed to establish the aerosol spectrum as follows:

$$\frac{dN}{d(\log D)} = \sum_{i=1}^n \frac{N_i}{\sqrt{2\pi}\log\sigma_i} \exp\left[-\frac{\log D - \log(D_g)}{2(\log\sigma_i)^2}\right] \quad (1)$$

where N_i is the aerosol number concentration in mode i , D is the particle diameter, D_g is the geometric mean diameter, and σ_i is the standard deviation (Li et al., 2015; Seinfeld and Pandis, 2016; Sun et al., 2013). Fig. 7 shows the best fits of the aerosol spectrum distant from the cloud, nearing the cloud, and at the cloud boundary. Table 2 lists the parameters used in Eq. (1) to characterize the aerosol size distribution in each zone.

3.3. Relative dispersion of the cloud droplet spectrum

It is well established that the shape of the cloud droplet spectrum, i. e., ϵ , is an important indicator characterizing cloud microphysical processes (Chandrakar et al., 2018; Liu et al., 2006c). As mentioned in the introduction, ϵ varies substantially in different clouds and has a certain correlation with N_c . However, some studies have reported an inconclusive correlation between ϵ and N_c (Xie and Liu, 2013). Here, the mean and maximum ϵ of the sampled cloud was 0.42 ± 0.13 and 0.81 , respectively. Fig. 8a shows that ϵ and N_c were negatively correlated. When N_c was low (e.g., $N_c < 50$ cm^{-3}), ϵ had a relatively large range (0.1 – 0.8). With increasing N_c , the range of ϵ values gradually decreased to 0.2 – 0.4 . The negative and converging relation of ϵ and N_c is similar to that reported by Zhao et al. (2006) and Deng et al. (2009). Also seen is a negative and converging correlation between ϵ and q_{Hotwire} (Fig. 8b). The range of spectral dispersion values narrowed as q_{Hotwire} increased (see also Fig. 8b). When $q_{\text{Hotwire}} > \sim 0.75$ g kg^{-1} , there was a significant negative correlation between ϵ and q_{Hotwire} . Wang et al. (2011) have indicated that ϵ is strongly related to the cloud droplet collision-coalescence process. More specifically, when $q_{\text{Hotwire}} < 0.75$ g kg^{-1} , updrafts and downdrafts were distributed irregularly, and ϵ varied over a wide range of values. When $q_{\text{Hotwire}} > 0.75$ g kg^{-1} , updrafts dominated, and ϵ tended to converge. Similar correlations were also obtained in an observational and modeling study (Tas et al., 2012). They considered that in the core region of a mature cumulus, the LWC is maximal and ϵ varies in a very narrow range. A strong negative correlation between ϵ and LWC is usually obtained in continental deep cumulus clouds (Ansari et al., 2020; Bera, 2021). Here, a similar result was seen in the convective core of the stratocumulus in this study. However, an airborne study made in the warm convective clouds near Istanbul show that for both inner clouds and their boundaries, the average ϵ remains almost constant with increasing LWC (Tas et al., 2015).

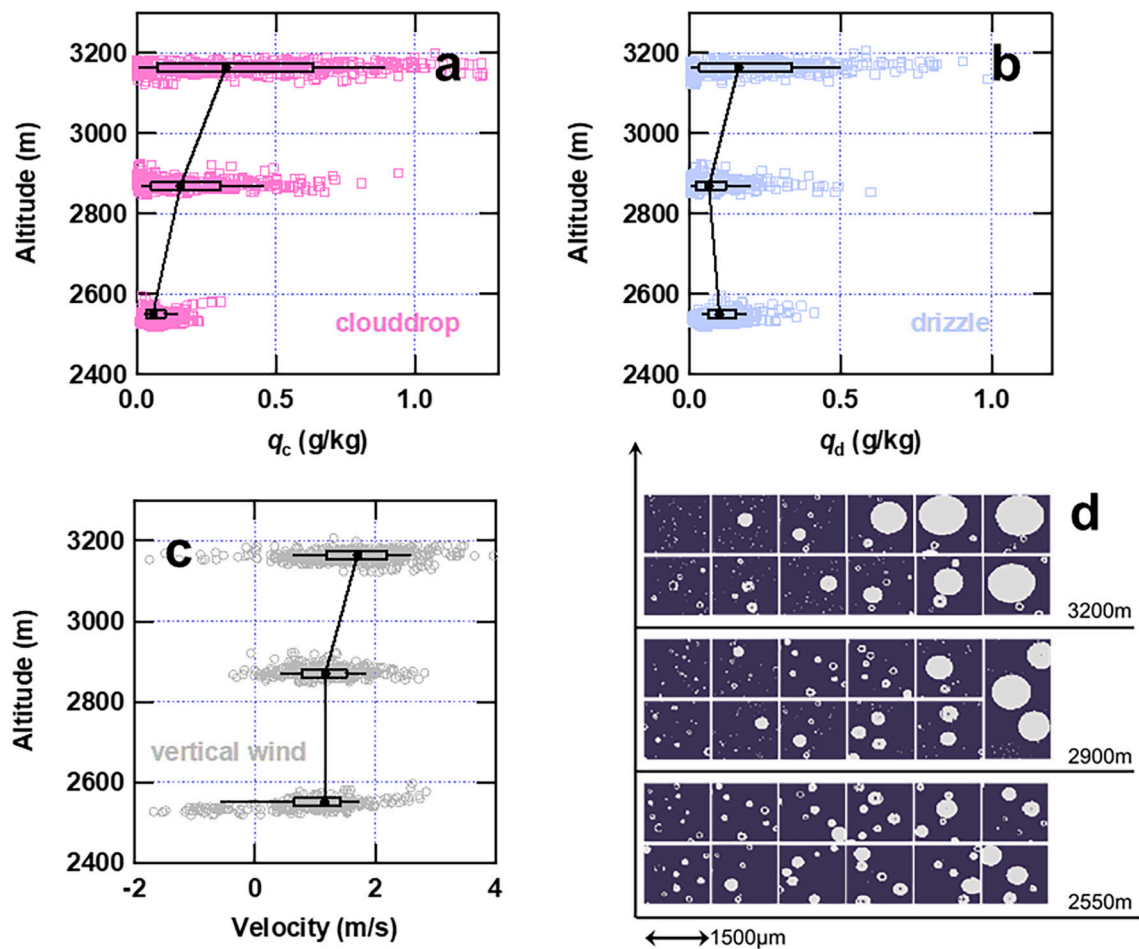


Fig. 5. Vertical variations of (a) the liquid water content of cloud droplets, (b) the liquid water content of drizzle drops, (c) vertical velocity during the three-level cloud sampling, and (d) CIP-measured 2D droplet images at levels I, II, and III in the case-study cloud. The boxes and whiskers represent the horizontal mean (solid circles), 25th and 75th percentiles (boxes), and 10th and 90th percentiles (left and right whiskers) of the data.

Some previous studies found that ϵ is roughly constant with height within a cloud (Martin et al., 1994; Nicholls and Leighton, 1986; Polivovich, 1993), while others showed that ϵ depends greatly on the cloud development stage (Tas et al., 2012). In particular, different environmental backgrounds and different cloud types may influence ϵ to varying degrees (Lu et al., 2007; Pawlowska et al., 2006). Fig. 9a and b show the ϵ of cloud droplets and drizzle drops at each horizontal level during cloud penetration. The mean cloud droplet ϵ increased by a factor of 2 from level I to level II then remained almost constant with height from level II to level III. Arabas et al. (2009) also reported similar results from observations made in marine cumuli during the Rain in Cumulus over the Ocean field experiment. In general, the mean drizzle drop ϵ increased with height from level I to level III, unlike the ϵ in non-drizzling clouds described by Martin et al. (1994) and Lu et al. (2007), which decreased or remained constant with height. From the previous discussion, this is likely related to the vertical distribution of cloud droplets and drizzle drops. Driven by updrafts, the mean $R_{e,d}$ increased due to the collision-coalescence and breakup of drizzle drops, but $R_{e,c}$ remained nearly constant. This caused the ϵ of drizzle drops to increase with altitude. At level III, possible aerosol washout by drizzle drops would enhance ϵ by reducing activated cloud droplets, accelerating the spectrum widening through increased drizzle. Different from our conclusion, some modeling studies have indicated that ϵ does not change with height significantly under lightly polluted conditions (Wang et al., 2011).

A negative correlation between ϵ and N_c was obtained at levels I and III during the period when the aircraft ascended through the cloud. The

slope of the negative relation between ϵ and N_c at the lower level of the cloud was steeper than that at the higher level of the cloud. A lower number concentration of cloud droplets ($N_c < 50 \text{ cm}^{-3}$) was measured at level I, with an ϵ value of ~ 0.15 corresponding to the maximum N_c at this level (Fig. 9f). The maximum N_c at level III was $\sim 200 \text{ cm}^{-3}$, with a corresponding ϵ value of ~ 0.3 (Fig. 9e). According to the definition of ϵ , when the ϵ value is relatively high, different sizes of cloud droplets are well mixed, easily triggering collision-coalescence and promoting the transformation of cloud droplets to raindrops. With decreasing ϵ , all droplets gradually approach the same size. The mean ϵ at level III was ~ 0.44 (Fig. 9e), slightly higher than at level I (mean $\epsilon \approx 0.38$). The maximum N_c value at level III corresponding to the mean ϵ value was also significantly higher than at level I. This suggests that the transformation from cloud water to rain was mainly from the middle and upper layers of the case-study cloud. The distribution of the cloud droplet spectrum then gradually narrowed during the raining process.

According to Xie and Liu (2013), the correlation between ϵ and N_c is complicated and difficult to describe with a simple mathematical expression. From the observational results reported by Liu et al. (2008) and Pandithurai et al. (2012), another variable related to the cloud droplet spectra was discussed, i.e., the specific cloud water content (γ), which represents the average water per droplet, defined as the ratio of the cloud LWC to N_c :

$$\gamma = \frac{L_c}{N_c} \quad (2)$$

where L_c is the cloud LWC. Here, CAS- and CIP-probe-measured droplet

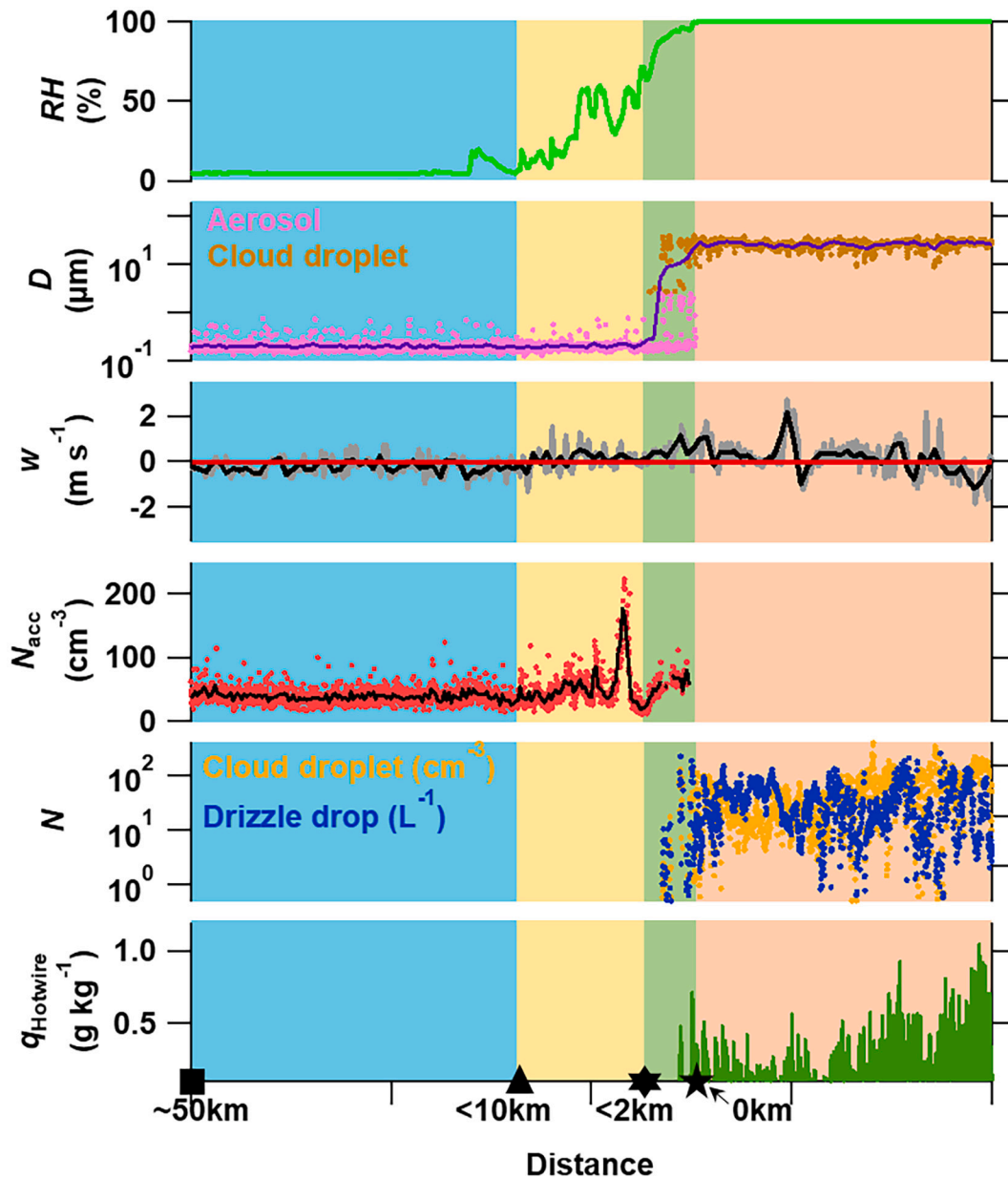


Fig. 6. Aircraft measurements before and during cloud penetration, showing (from top to bottom) relative humidity (RH); size distribution of pre-cloud aerosols (pink dots) and cloud droplets (orange dots); 1-Hz vertical velocity (w) and 10-s mean w , where the red line indicates $w = 0 \text{ m s}^{-1}$; ambient and pre-cloud accumulation-mode aerosol concentrations (N_{acc}), where the black line shows 5-s averaged N_{acc} ; cloud droplet (orange dots, unit: cm^{-3}) and drizzle drop (blue dots, unit: L^{-1}) number concentrations; and cloud water mixing ratio (q_{Hotwire}) measured by the Hotwire probe. Data in this figure correspond to the time period outlined by the red dashed box in Fig. 3. The region is split up into four zones: distant from the cloud (blue), nearing the cloud (yellow), at the cloud boundary (green), and inside the cloud (orange). The black marks on the abscissa represent horizontal distances to the cloud boundary ($RH = 100\%$), also shown in Fig. 1b. (For interpretation of the references to colour in this figure legend, the reader is referred to the web version of this article.)

water contents were used to represent cloud droplet and drizzle L_c , respectively. The average cloud droplet γ was $6.48 \pm 3.13 \text{ ng}$ during cloud penetration. Values of γ varied greatly along the same level of the cloud. However, in the vertical, the mean γ was relatively constant with height (Fig. 9c).

Most GCMs use a proportionality factor β to represent the spectral shape of a cloud droplet size distribution (Rotstajn and Liu, 2009; Xie et al., 2017). According to Lohmann and Roeckner (1996), β is a dimensionless parameter, also called the effective radius ratio, expressed as:

$$\beta = \frac{R_c}{R_v} \tag{3}$$

where R_v is the mean volume radius of cloud droplets. Many airborne observations indicate that β can be approximated as a constant value [e.g., $\beta = 1.14$ by Martin et al., 1994, $\beta = 1.22$ by Deng et al., 2009, and $\beta = 1.18$ by Pandithurai et al., 2012] and is an increasing function of ϵ (Liu and Daum, 2002). Here, β was calculated using aircraft penetration data from the marine stratocumulus cloud studied. Fig. 10 shows the scatterplot of R_c as a function of R_v from the cloud penetration data. The slope from linear regression is 1.16 (correlation coefficient = 0.97), indicating that β can be regarded as a constant value. Taking ϵ into consideration, large ϵ values correspond to a larger slope, and small ϵ values indicate that β is close to unity ($\beta = 1$ for a monodispersed droplet size distribution).

The coefficient $k = \beta^{-3}$ is a parameter that relates R_c and R_v in GCMs

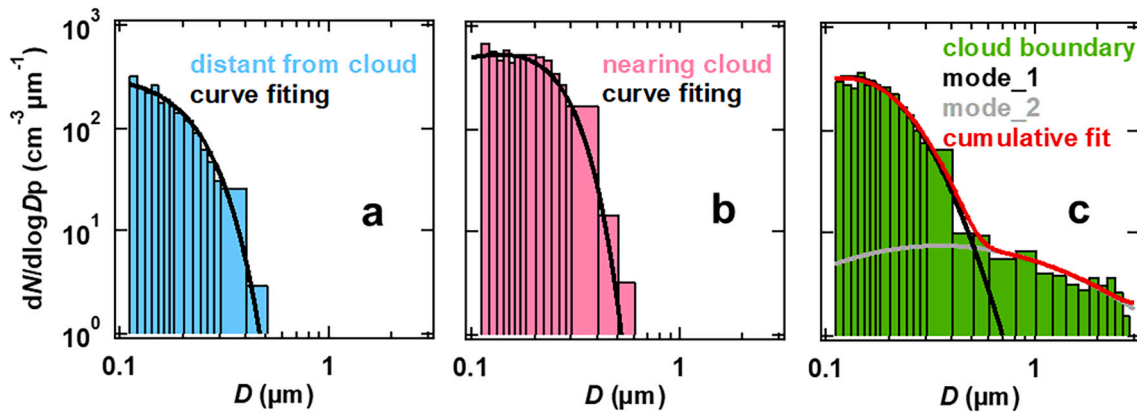


Fig. 7. Mean size distributions of accumulation-mode aerosols (a) distant from the cloud, (b) nearing the cloud, and (c) at the cloud boundary. The black lines show the mono-lognormal fits of the aerosol size distribution, and the gray line in (c) shows the multi-lognormal fit. The mono- and multi-lognormal fits in (c) are denoted as “mode 1” and “mode 2”, respectively, in Table 2. The red line in (c) shows the cumulative fit of the aerosol size distribution at the cloud boundary. (For interpretation of the references to colour in this figure legend, the reader is referred to the web version of this article.)

Table 2

Fitting parameters characterizing the lognormal size distribution of accumulation-mode aerosols in different zones before cloud penetration.

Phase	Mode 1			Mode 2		
	N_{acc} (cm^{-3})	D_g (μm)	\log (σ)	N_{acc} (cm^{-3})	D_g (μm)	\log (σ)
Distant from the cloud	286	0.11	0.65	0		
Nearing the cloud	530	0.17	0.5	0		
At the cloud boundary	290	0.13	0.7	7.9	1.31	1.8

(Chandrakar et al., 2018; Ovtchinnikov and Ghan, 2005). The k value measured in this study was inversely proportional to ϵ , which is also in agreement with observations made in warm stratocumulus clouds (Lu and Seinfeld, 2006). Compared with polluted continental cumuli, clean maritime clouds have larger k values. The mean k in this study was ~ 0.64 , slightly higher than the mean value of k measured in Indian continental cumuli (Pandithurai et al., 2012) and lower than that in eastern Pacific coastal marine stratocumulus clouds (Lu et al., 2008).

The parameter β can also be parameterized by establishing a

relationship between ϵ and β . According to previous research on cloud microphysical schemes in GCMs, lognormal, gamma, and Weibull distribution functions are most commonly used. According to the detailed analysis presented in the supplement, the lognormal, gamma, and Weibull distributions are, in general, more suitable for fitting the cloud droplet spectrum but can also be used to fit the drizzle drop spectrum for values of $\epsilon < 0.5$.

3.4. Cloud droplet dispersion effect on the R_e parameterization and the Twomey indirect effect

Assuming a constant β for the cloud effective radius parameterization has been a common practice used for evaluating the IE (Pandithurai et al., 2012). Since R_v can be expressed as

$$R_v = \left(\frac{3}{4\pi\rho} \frac{L_c}{N_c} \right)^{\frac{1}{3}} \quad (4)$$

and using Eq. (3), R_e can be expressed as

$$R_e = \beta \left(\frac{3}{4\pi\rho} \frac{L_c}{N_c} \right)^{\frac{1}{3}} \quad (5)$$

Since N_c and L_c are both predictable variables, R_e is parameterized

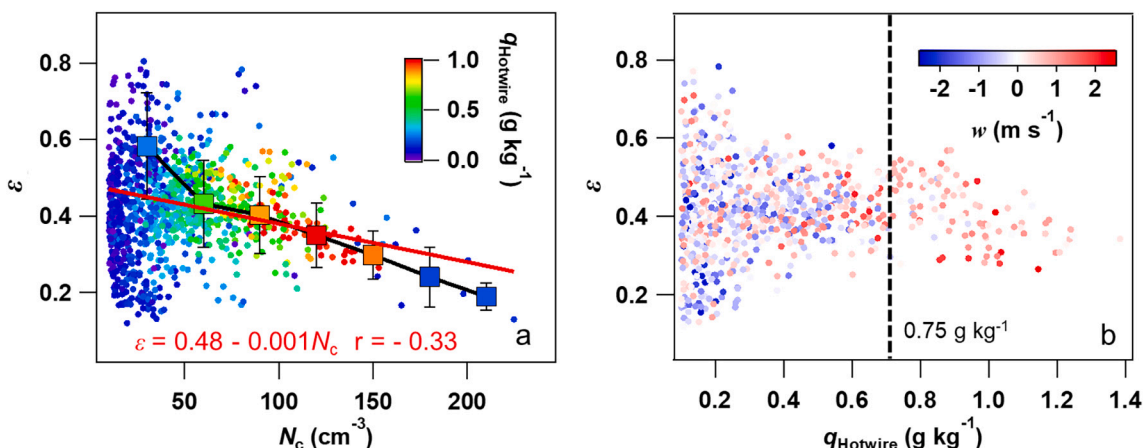


Fig. 8. (a) Relative dispersion (ϵ) as a function cloud droplet number concentration (N_c), with colors representing the cloud water mixing ratio measured by the Hotwire probe ($q_{Hotwire}$), and (b) ϵ as a function of $q_{Hotwire}$, with colors representing the vertical velocity (w). Error bars in the left panel represent the standard deviation of average ϵ in each 30 cm^{-3} cloud droplet concentration bin, and the red line represents the best fit. The red and blue dots in the right panel represent updrafts and downdrafts, respectively, within the cloud, and the dashed line shows $q_{Hotwire} = 0.75\text{ g kg}^{-1}$. (For interpretation of the references to colour in this figure legend, the reader is referred to the web version of this article.)

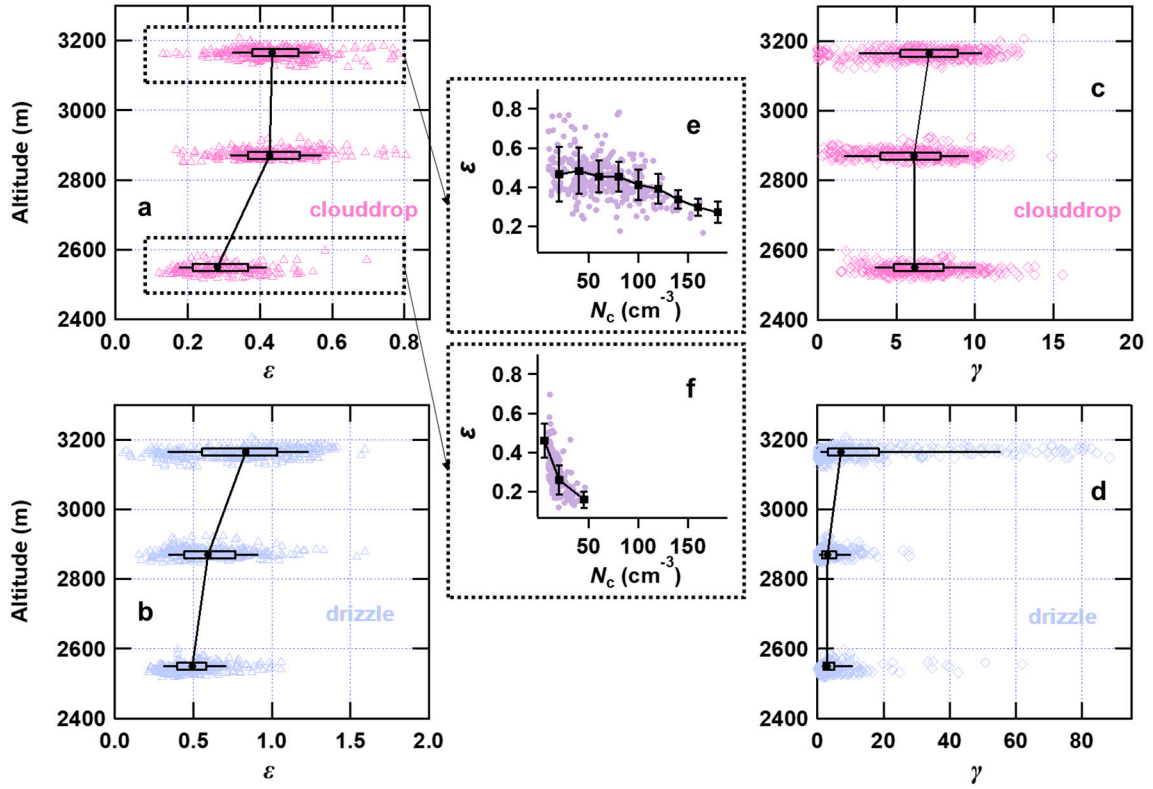


Fig. 9. Box-and-whiskers plots of (a) cloud droplet spectral dispersion, (b) drizzle drop spectral dispersion, (c) specific cloud water content (ng), and (d) specific drizzle water content (μg). The bottom and top of each box represent the 25th and 75th percentiles, the left and right whiskers represent the 10th and 90th percentiles, and the solid circles represent the horizontal means of the data. The correlation between dispersion and cloud droplet number concentration (N_c) at (e) level III and (f) level I in the case-study cloud are also shown.

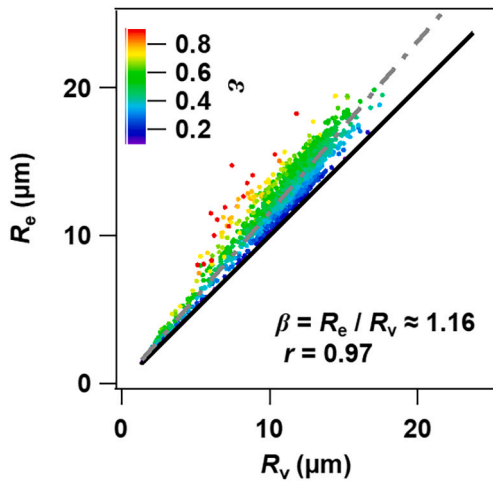


Fig. 10. Cloud droplet effective radius (R_e) as a function of mean volume radius (R_v), with colors representing the relative dispersion (ϵ). The gray dot-dash line is the best-fit line from linear regression, and the black line is the 1:1 line. The linear fit y-intercept is forced with zero, and the slope, representing the effective radius ratio (β), is 1.16 (correlation coefficient, $r = 0.97$).

according to Eq. (5) in many GCMs. Fig. 11a shows the dependence of γ on R_e , R_m , and R_v so that the dispersion effect on the cloud droplet size distribution can be examined. Also shown is the curve describing the radius- γ relation of a pure water droplet. For a given γ , $R_e > R_v > R_m$. Note that the R_v - γ curve can represent the water content of pure water droplets. Applying the gamma distribution function to Eq. (S1), ϵ is introduced to the R_e parameterization:

$$R_e = \frac{(1 + 2\epsilon^2)^{\frac{3}{2}}}{(1 + \epsilon^2)^{\frac{1}{2}}} \left(\frac{3}{4\pi\rho} \frac{L_c}{N_c} \right)^{\frac{1}{3}} \quad (6)$$

If $\epsilon = 0$, then $R_e = R_v$. As ϵ increases, R_e increases more than R_v . So, ϵ can further affect indirect forcing by changing the R_e distribution in a cloud (Xie et al., 2013).

The IE is difficult to quantify because it not only depends on the interactions between aerosols and clouds but is also affected by meteorology. The dependence of N_c or R_e on aerosol amount can characterize IE (Shao and Liu, 2009). Furthermore, aerosol amount in IE characterization can be N_{acc} (Feingold et al., 2001), aerosol light scattering (Garrett et al., 2004; Kim et al., 2003), aerosol optical depth (Yuan et al., 2008), cloud condensation nuclei (Zhao et al., 2012), $\text{PM}_{2.5}$, and so on. Here, N_{acc} is used instead of aerosol amount. According to Feingold et al. (2001, 2003) and Garrett et al. (2004), IE can be quantified using the following expressions:

$$IE_n = \frac{1}{3} \frac{\Delta \log N_c}{\Delta \log N_{acc}}, \text{ and } IE_s = - \frac{\Delta \log R_e}{\Delta \log N_{acc}} \quad (7)$$

where $\Delta \log N_{acc}$ is the relative change in sub-cloud aerosols. Variations in aerosols outside of the cloud near its lateral boundary are used here as a substitute. IE_n and IE_s represent the first IE in terms of the number and size effects, respectively. Recent studies have found that the dispersion effect may offset the Twomey effect (Liu et al., 2008; Rotstayn and Liu, 2003), with the resultant IE an algebraic sum of both Twomey and dispersion effects. It can simply be expressed as $IE = IE_n + DE$, where DE is the offset Twomey effect associated with the increment in ϵ (Liu et al., 2008).

Based on the aerosol-cloud interaction studies by Kaufman and Fraser (1997) and Nakajima et al. (2001), the correlation between N_{acc} and N_c can be expressed as

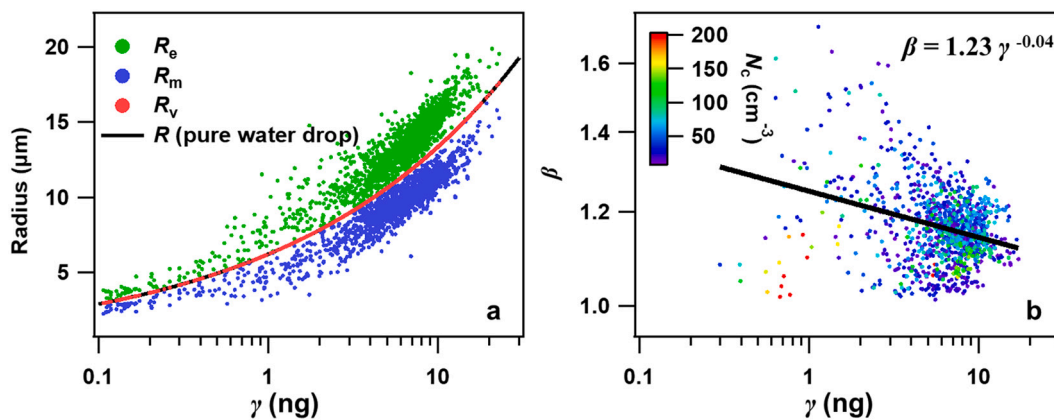


Fig. 11. (a) Scatterplot showing the dependence of cloud droplet effective radius (R_e), mean radius (R_m), and mean volume radius (R_v) on specific cloud water content (γ). Also shown is the calculated pure water drop radius (black curve). (b) Relation between effective radius ratio (β) and γ , with colors representing cloud droplet number concentration (N_c). The black line is the best-fit line from linear regression between $\log \beta$ and $\log \gamma$. The best-fit power function is given in the upper right corner.

$$N_c = aN_{acc}^b \quad (8)$$

Here, a is a constant, and b is the exponent to the power-law fit between N_{acc} and N_c (Pandithurai et al., 2012). According to Eqs. (7) and (8), IE_n is approximately equal to $b/3$. Fig. 12a shows the dependence of N_c on the pre-cloud N_{acc} . Here, N_c increased as N_{acc} increased, with a correlation coefficient of ~ 0.62 . The exponent b is ~ 0.26 , indicating that IE_n in this study is ~ 0.087 . Similar relations were also reported by Lu et al. (2008) and Pandithurai et al. (2012), although a and b were slightly different. With the exception of N_c , the variation in R_e caused by pre-cloud aerosols is also an indicator of the first IE. Fig. 12b shows R_e as a function of N_{acc} . R_e slightly decreased as N_{acc} increased, with a negative correlation coefficient of ~ 0.48 . The slope of the linear fit to the log-log plot is -0.084 , which by Eq. (7) is IE_s . Unlike N_c and N_{acc} used to calculate IE_n , which does not account for the influence of dispersion, IE_s estimated from R_e and N_{acc} is likely affected by the cloud droplet DE.

The complex relationship between ε (or β) and N_c incurs large uncertainties in the estimation of DE. Liu et al. (2006b) used γ as a proxy variable and proposed a β - γ parameterization scheme. The dependence of β on γ can be parameterized as

$$\beta = \alpha_\beta \gamma^{-b_\beta} \quad (9)$$

where α_β is a constant, and b_β is the dispersion factor, obtained from the linear fit between $\log \beta$ and $\log \gamma$. According to Liu et al. (2008), the exponent b_β is defined as the percentage of offset or enhancement to the

Twomey cooling effect due to the shape of the cloud droplet spectrum. A b_β value of 0.1 denotes a DE offsetting IE_n by $\sim 30\%$. Fig. 11b shows that $\log \beta$ is negatively correlated with $\log \gamma$, independent of N_c . The empirical relation is $\beta = 1.23 \gamma^{-0.04}$. Pandithurai et al. (2012) reported that $\beta = 0.067 \gamma^{-0.13}$ based on observations from continental cumuli over India. Liu et al. (2008) found that $\beta = 0.07 \gamma^{-0.14}$ based on aircraft observations from different field campaigns. However, Martins and Silva Dias (2009) reported that β increased as γ increased based on data from a biomass burning season in the Amazon. Here, using $b_\beta = 0.04$, DE may offset the Twomey effect by $(0.04 / 0.1) \times 30\% \approx 12\%$ in the case-study cloud. DE is also associated with the enhancement of ε , calculated as $DE = -b_\beta b = -0.04 \times 0.26 \approx -0.01$. Considering the dispersion effect, the quantitative estimate of IE in this study is $IE_n + DE \approx 0.077$. The resultant IE is slightly greater than IE_s (0.084), which was estimated using parameterized R_e , suggesting that including DE in the IE estimation for the stratocumulus cloud in this study does not contribute much. Previous studies on estimating the IE in polluted and non-drizzling clouds report a greater contribution of DE to the IE (Anil Kumar et al., 2016; Pandithurai et al., 2012). However, note that these conclusions were based on the result of single-flight measurements. The large biases in cloud properties seen in Fig. 12a and b also suggest a large uncertainty in the IE estimation under low N_c and drizzling conditions.

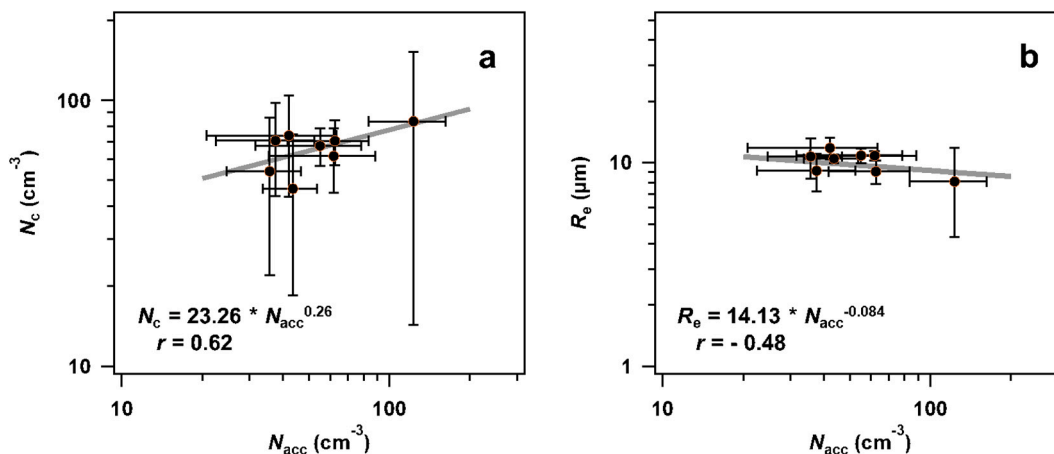


Fig. 12. (a) Cloud droplet number concentration (N_c) and (b) effective radius (R_e) as a function of pre-cloud aerosol concentration (N_{acc}). Error bars show the standard deviations of the data. The gray lines and power functions represent the best fits. Correlation coefficients (r) are also given.

4. Conclusions

This study mainly focused on aircraft observations of a drizzling marine stratocumulus cloud deck over the eastern coast of China. Examined were cloud microphysical characteristics, aerosol-cloud interactions, and dispersion and indirect effects. Note that the conclusions presented here are based on measurements made during a single flight and that the parameterization and estimation of *IE* may only be applicable to drizzling marine stratocumulus over coastal regions.

Large sizes and low concentrations of cloud and drizzle droplets were observed during cloud penetration, and clear differences were demonstrated through a detailed analysis of the vertical distributions of cloud parameters. The collision and coalescence of cloud droplets and drizzle drops, the condensation of small droplets, and the collision-induced break-up of drizzle drops were considered to be the primary microphysical processes in the cloud under study. By analyzing ambient atmospheric, aerosol, and cloud properties in the vicinity of the cloud lateral boundary, the interaction between aerosol particles and cloud droplets was discussed. Defined were two zones between the region distant from the cloud and inside the cloud, i.e., the transition zone (where aerosols neared the cloud) and the lateral boundary zone. The increase in transition-zone N_{acc} and the enlargement of lateral-boundary-zone particles were likely due to the entrainment and mixing of dry air and cloud droplet evaporation. Also shown were the spectra of accumulation-mode aerosols in the zone distant from the cloud, in the transition zone, and in the lateral boundary zone. A lognormal function was used to fit the aerosol number size distribution.

Different from some previous studies, a negative relation between averaged ε and N_c was found for the cloud under study. Furthermore, ε was closely related to $q_{Hotwire}$ and w . When $q_{Hotwire}$ was greater than 0.75 g kg^{-1} , updrafts dominated, and ε tended to converge. This is probably because the analyzed data was acquired from the core region of the mature cumulus, where updrafts and $q_{Hotwire}$ reach their maximum and where ε has a very narrow range of values. Unlike non-drizzling stratocumulus clouds, which have a relative dispersion almost constant with height, the cloud droplet and drizzle drop spectral dispersions increased with height in the case-study cloud. As an important input to the parameterization scheme of a cloud model, the value of β was ~ 1.16 . The gamma and lognormal distributions best described the relationship between ε and parameterized β .

Introducing ε into the R_e parameterization can further affect the indirect forcing by changing the R_e distribution inside the cloud. The *DE* was estimated using β and γ , with an in-depth analysis indicating that *DE* may offset the Twomey effect by $\sim 12\%$ for the cloud examined in this study. The dependence of N_{acc} on N_c and N_{acc} on R_e was used to calculate the *IE*. The calculation also considered the estimated *IE* offset by *DE*. Two different methods of estimating *IE* yielded close values (0.084 and 0.077), suggesting that for the drizzling marine stratocumulus cloud studied here, introducing *DE* into the estimation of *IE* had little influence. Note that the estimated *IE* has a large uncertainty, given the large biases in the cloud properties measured.

Author statement

Fei Wang and Xincheng Ma designed the aircraft campaign. Delong Zhao, Yang Gao, Jiujiang Sheng, and Ping Tian performed experiments. Fei Wang analyzed the airborne data. Fei Wang, Zhanqing Li, and Cribb Maureen wrote the paper.

Data availability

Data is available upon request from Fei Wang (feiwang@cma.gov.cn).

Declaration of Competing Interest

The authors declare that they have no known competing financial interests or personal relationships that could have appeared to influence the work reported in this paper.

Acknowledgements

This study was supported by the National Natural Science Foundation of China (42030606). We are very grateful to the reviewers for their constructive comments and thoughtful suggestions. We also thank all of the experimental research team, especially the flight crew of the Beijing Y-12 airplane.

Appendix A. Supplementary data

Supplementary data to this article can be found online at <https://doi.org/10.1016/j.atmosres.2021.105885>.

References

- Albrecht, B.A., 1989. Aerosols, cloud microphysics, and fractional cloudiness. *Science* 245, 1227–1231.
- Anil Kumar, V., et al., 2016. Investigation of aerosol indirect effects on monsoon clouds using ground-based measurements over a high-altitude site in Western Ghats. *Atmos. Chem. Phys.* 16, 8423–8430.
- Ansari, K., Pandithurai, G., Anil Kumar, V., 2020. Role of droplet size classes on the cloud droplet spectral dispersion as observed over the Western Ghats. *Atmos. Res.* 246, 105104.
- Arabas, S., Pawlowska, H., Grabowski, W., 2009. Effective radius and droplet spectral width from in-situ aircraft observations in trade-wind cumuli during RICO. *Geophys. Res. Lett.* 36.
- Baumgardner, D., Jonsson, H., Dawson, W., O'Connor, D., Newton, R., 2001. The cloud, aerosol and precipitation spectrometer: a new instrument for cloud investigations. *Atmos. Res.* 59–60, 251–264.
- Bera, S., 2021. Droplet spectral dispersion by lateral mixing process in continental deep cumulus clouds. *J. Atmos. Sol. Terr. Phys.* 214, 105550.
- Brenguier, J.-L., Burnet, F., Geoffroy, O., 2011. Cloud optical thickness and liquid water path - does the k coefficient vary with droplet concentration? *Atmos. Chem. Phys.* 11, 9771–9786.
- Burnet, F., Brenguier, J.-L., 2007. Observational study of the entrainment-mixing process in warm convective clouds. *J. Atmos. Sci.* 64, 1995–2011.
- Cecchini, M.A., et al., 2017. Sensitivities of Amazonian clouds to aerosols and updraft speed. *Atmos. Chem. Phys.* 10037–10050.
- Chandrakar, K.K., et al., 2016. Aerosol indirect effect from turbulence-induced broadening of cloud-droplet size distributions. *Proc. Natl. Acad. Sci.* 113, 14243–14248.
- Chandrakar, K.K., Cantrell, W., Kostinski, A.B., Shaw, R.A., 2018. Dispersion aerosol indirect effect in turbulent clouds: laboratory measurements of effective radius. *Geophys. Res. Lett.* 45, 10738–10745.
- Chen, S., Yau, M.-K., Bartello, P., Xue, L., 2018a. Bridging the condensation–collision size gap: a direct numerical simulation of continuous droplet growth in turbulent clouds. *Atmos. Chem. Phys.* 18.
- Chen, S., Yau, M., Bartello, P., 2018b. Turbulence effects of collision efficiency and broadening of droplet size distribution in cumulus clouds. *J. Atmos. Sci.* 75, 203–217.
- De Rooy, W.C., et al., 2013. Entrainment and detrainment in cumulus convection: an overview. *Q. J. R. Meteorol. Soc.* 139, 1–19.
- Deng, Z., Zhao, C., Zhang, Q., Huang, M., Ma, X., 2009. Statistical analysis of microphysical properties and the parameterization of effective radius of warm clouds in Beijing area. *Atmos. Res.* 93, 888–896.
- Desai, N., Chandrakar, K., Chang, K., Cantrell, W., Shaw, R., 2018. Influence of microphysical variability on stochastic condensation in a turbulent laboratory cloud. *J. Atmos. Sci.* 75, 189–201.
- Desai, N., Glienke, S., Fugal, J., Shaw, R.A., 2019. Search for microphysical signatures of stochastic condensation in marine boundary layer clouds using airborne digital holography. *J. Geophys. Res.-Atmos.* 124, 2739–2752.
- Feingold, G., Remer, L.A., Ramaprasad, J., Kaufman, Y.J., 2001. Analysis of smoke impact on clouds in Brazilian biomass burning regions: an extension of Twomey's approach. *J. Geophys. Res.-Atmos.* 106, 22907–22922.
- Feingold, G., Eberhard, W.L., Veron, D.E., Previdi, M., 2003. First measurements of the Twomey indirect effect using ground-based remote sensors. *Geophys. Res. Lett.* 30.
- Garrett, T., Zhao, C., Dong, X., Mace, G., Hobbs, P., 2004. Effects of varying aerosol regimes on low-level Arctic stratus. *Geophys. Res. Lett.* 31.
- Ghan, S.J., et al., 2001. A physically based estimate of radiative forcing by anthropogenic sulfate aerosol. *J. Geophys. Res.-Atmos.* 106, 5279–5293.
- Grabowski, W.W., Pawlowska, H., 1993. Entrainment and mixing in clouds: the Paluch mixing diagram revisited. *J. Appl. Meteorol.* 32, 1767–1773.
- Grandey, B., Stier, P., 2010. A critical look at spatial scale choices in satellite-based aerosol indirect effect studies. *Atmos. Chem. Phys.* 10, 11459–11470.

- Kaufman, Y.J., Fraser, R.S., 1997. The effect of smoke particles on clouds and climate forcing. *Science* 277, 1636–1639.
- Kim, B.G., Schwartz, S.E., Miller, M.A., Min, Q., 2003. Effective radius of cloud droplets by ground-based remote sensing: Relationship to aerosol. *J. Geophys. Res.-Atmos.* 108.
- King, M.D., Platnick, S., Menzel, W.P., Ackerman, S.A., Hubanks, P.A., 2013. Spatial and temporal distribution of clouds observed by MODIS onboard the Terra and Aqua satellites. *IEEE Trans. Geosci. Remote Sens.* 51, 3826–3852.
- Kleinman, L.L., et al., 2012. Aerosol concentration and size distribution measured below, in, and above cloud from the DOE G-1 during VOCALS-REx. *Atmos. Chem. Phys.* 12, 207–223.
- Lance, S., 2012. Coincidence errors in a cloud droplet probe (CDP) and a cloud and aerosol spectrometer (CAS), and the improved performance of a modified CDP. *J. Atmos. Ocean. Technol.* 29, 1532–1541.
- Li, J., et al., 2015. Aircraft measurements of the vertical distribution and activation property of aerosol particles over the Loess Plateau in China. *Atmos. Res.* 155, 73–86.
- Li, Z., et al., 2016. Aerosol and monsoon climate interactions over Asia. *Rev. Geophys.* 54, 866–929.
- Li, Z., Rosenfeld, D., Fan, J., 2017. Aerosols and their impact on radiation, clouds, precipitation, and severe weather events. *Oxford Res. Encyclopedia Environ. Sci.* <https://doi.org/10.1093/acrefore/9780199389414.013.126>.
- Li, Z., et al., 2019. East asian study of tropospheric aerosols and their impact on regional clouds, precipitation, and climate (EAST-AIRCPC). *J. Geophys. Res.-Atmos.* 124, 13026–13054.
- Liu, Y., Daum, P.H., 2002. Anthropogenic aerosols: indirect warming effect from dispersion forcing. *Nature* 419, 580–581.
- Liu, Y., Daum, P.H., McGraw, R., Miller, M., 2006a. Generalized threshold function accounting for effect of relative dispersion on threshold behavior of autoconversion process. *Geophys. Res. Lett.* 33.
- Liu, Y., Daum, P.H., McGraw, R., Wood, R., 2006b. Parameterization of the autoconversion process. Part II: Generalization of Sundqvist-type parameterizations. *J. Atmos. Sci.* 63, 1103–1109.
- Liu, Y., Daum, P.H., Yum, S.S., 2006c. Analytical expression for the relative dispersion of the cloud droplet size distribution. *Geophys. Res. Lett.* 33.
- Liu, Y., Daum, P.H., Guo, H., Peng, Y., 2008. Dispersion bias, dispersion effect, and the aerosol–cloud conundrum. *Environ. Res. Lett.* 3, 045021.
- Lohmann, U., Roeckner, E., 1996. Design and performance of a new cloud microphysics scheme developed for the ECHAM general circulation model. *Clim. Dyn.* 12, 557–572.
- Lu, M.L., Seinfeld, J.H., 2006. Effect of aerosol number concentration on cloud droplet dispersion: A large-eddy simulation study and implications for aerosol indirect forcing. *J. Geophys. Res.-Atmos.* 111.
- Lu, M.-L., et al., 2007. The Marine Stratatus/Stratocumulus Experiment (MASE): Aerosol-cloud relationships in marine stratocumulus. *J. Geophys. Res.-Atmos.* 112.
- Lu, M.-L., et al., 2008. Aerosol-cloud relationships in continental shallow cumulus. *J. Geophys. Res.-Atmos.* 113.
- Lu, C., Liu, Y., Niu, S., Vogelmann, A.M., 2012a. Observed impacts of vertical velocity on cloud microphysics and implications for aerosol indirect effects. *Geophys. Res. Lett.* 39.
- Lu, C., Liu, Y., Yum, S.S., Niu, S., Endo, S., 2012b. A new approach for estimating entrainment rate in cumulus clouds. *Geophys. Res. Lett.* 39.
- Lu, C., et al., 2020. Reconciling contrasting relationships between relative dispersion and volume-mean radius of cloud droplet size distributions. *J. Geophys. Res.-Atmos.* 125 (p. e2019JD031868).
- Ma, J., et al., 2010. Strong air pollution causes widespread haze-clouds over China. *J. Geophys. Res.-Atmos.* 115.
- Martin, G., Johnson, D., Spice, A., 1994. The measurement and parameterization of effective radius of droplets in warm stratocumulus clouds. *J. Atmos. Sci.* 51, 1823–1842.
- Martins, J.A., Silva Dias, M.A.F., 2009. The impact of smoke from forest fires on the spectral dispersion of cloud droplet size distributions in the Amazonian region. *Environ. Res. Lett.* 4, 015002.
- Nakajima, T., Higurashi, A., Kawamoto, K., Penner, J.E., 2001. A possible correlation between satellite-derived cloud and aerosol microphysical parameters. *Geophys. Res. Lett.* 28, 1171–1174.
- Nicholls, S., Leighton, J., 1986. An observational study of the structure of stratiform cloud sheets: part I. Structure. *Q. J. R. Meteorol. Soc.* 112, 431–460.
- Ovtchinnikov, M., Ghan, S.J., 2005. Parallel simulations of aerosol influence on clouds using cloud-resolving and single-column models. *J. Geophys. Res.-Atmos.* 110.
- Pandithurai, G., et al., 2012. Aerosol effect on droplet spectral dispersion in warm continental cumuli. *J. Geophys. Res.-Atmos.* 117.
- Pardo, L.H., et al., 2021. Observed and simulated variability of droplet spectral dispersion in convective clouds over the Amazon. *J. Geophys. Res.-Atmos.* <https://doi.org/10.1029/2021JD035076>.
- Pawlowska, H., Grabowski, W.W., Brenguier, J.L., 2006. Observations of the width of cloud droplet spectra in stratocumulus. *Geophys. Res. Lett.* 33.
- Peng, Y., Lohmann, U., 2003. Sensitivity study of the spectral dispersion of the cloud droplet size distribution on the indirect aerosol effect. *Geophys. Res. Lett.* 30.
- Politovich, M.K., 1993. A study of the broadening of droplet size distributions in cumuli. *J. Atmos. Sci.* 50, 2230–2244.
- Prabha, T.V., et al., 2012. Spectral width of premonsoon and monsoon clouds over Indo-Gangetic valley. *J. Geophys. Res.-Atmos.* 117.
- Pruppacher, H.R., Klett, J.D., 2012. *Microphysics of Clouds and Precipitation: Reprinted 1980*. Springer Science & Business Media.
- Qiu, Y., Zhao, C., Guo, J., Li, J., 2017. 8-Year ground-based observational analysis about the seasonal variation of the aerosol-cloud droplet effective radius relationship at SGP site. *Atmos. Environ.* 164, 139–146.
- Rosenfeld, D., Gutman, G., 1994. Retrieving microphysical properties near the tops of potential rain clouds by multispectral analysis of AVHRR data. *Atmos. Res.* 34, 259–283.
- Rosenfeld, D., Lensky, I.M., 1998. Satellite-based insights into precipitation formation processes in continental and maritime convective clouds. *Bull. Am. Meteorol. Soc.* 79, 2457–2476.
- Rotstaysn, L.D., Liu, Y., 2003. Sensitivity of the first indirect aerosol effect to an increase of cloud droplet spectral dispersion with droplet number concentration. *J. Clim.* 16, 3476–3481.
- Rotstaysn, L.D., Liu, Y., 2009. Cloud droplet spectral dispersion and the indirect aerosol effect: Comparison of two treatments in a GCM. *Geophys. Res. Lett.* 36.
- Seinfeld, J.H., Pandis, S.N., 2016. *Atmospheric Chemistry and Physics: From Air Pollution to Climate Change*. John Wiley & Sons.
- Shao, H., Liu, G., 2009. A critical Examination of the Observed first Aerosol indirect effect. *J. Atmos. Sci.* 66, 1018–1032.
- Stommel, H., 1947. Entrainment of air into a cumulus cloud: (Paper presented 27 December 1946 at the Annual Meeting, AMS, Cambridge, Massachusetts). *J. Meteorol.* 4, 91–94.
- Sun, X., et al., 2013. Seasonal and vertical variations in aerosol distribution over Shijiazhuang, China. *Atmos. Environ.* 81, 245–252.
- Tas, E., Koren, I., Altaratz, O., 2012. On the sensitivity of droplet size relative dispersion to warm cumulus cloud evolution. *Geophys. Res. Lett.* 3 (9).
- Tas, E., et al., 2015. The relative dispersion of cloud droplets: its robustness with respect to key cloud properties. *Atmos. Chem. Phys.* 15, 2009.
- Terai, C., Bretherton, C., Wood, R., Painter, G., 2014. Aircraft observations of aerosol, cloud, precipitation, and boundary layer properties in pockets of open cells over the Southeast Pacific. *Atmos. Chem. Phys.* 14, 8071–8088.
- Tölle, M.H., Krueger, S.K., 2014. Effects of entrainment and mixing on droplet size distributions in warm cumulus clouds. *J. Adv. Model. Earth Syst.* 6, 281–299.
- Twomey, S., 1974. Pollution and the planetary albedo. *Atmos. Environ.* 8, 1251–1256.
- Wang, X., Xue, H., Fang, W., Zheng, G., 2011. A study of shallow cumulus cloud droplet dispersion by large eddy simulations. *Acta Meteorol. Sin.* 25, 166–175.
- Wang, F., et al., 2019. Evaluation of hygroscopic cloud seeding in liquid-water clouds: a feasibility study. *Atmos. Chem. Phys.* 19, 14967–14977.
- Wang, Y., et al., 2021. Dispersion of droplet size distributions in supercooled non-precipitating stratocumulus from aircraft observations obtained during the southern ocean cloud radiation aerosol transport experimental study. *J. Geophys. Res.-Atmos.* 126 (p. e2020JD033720).
- Wood, R., 2012. Stratocumulus Clouds. *Mon. Weather Rev.* 140, 2373–2423.
- Xie, X., Liu, X., 2009. Analytical three-moment autoconversion parameterization based on generalized gamma distribution. *J. Geophys. Res.-Atmos.* 114.
- Xie, X., Liu, X., 2011. Effects of spectral dispersion on clouds and precipitation in mesoscale convective systems. *J. Geophys. Res.-Atmos.* 116.
- Xie, X., Liu, X., 2013. Analytical studies of the cloud droplet spectral dispersion influence on the first indirect aerosol effect. *Adv. Atmos. Sci.* 30, 1313–1319.
- Xie, X., et al., 2013. Numerical simulation of clouds and precipitation depending on different relationships between aerosol and cloud droplet spectral dispersion. *Tellus Ser. B Chem. Phys. Meteorol.* 65, 19054.
- Xie, X., Zhang, H., Liu, X., Peng, Y., Liu, Y., 2017. Sensitivity study of cloud parameterizations with relative dispersion in CAM5.1: impacts on aerosol indirect effects. *Atmos. Chem. Phys.* 17, 5877–5892.
- Yuan, T., Li, Z., Zhang, R., Fan, J., 2008. Increase of cloud droplet size with aerosol optical depth: An observation and modeling study. *J. Geophys. Res.-Atmos.* 113.
- Yum, S.S., Hudson, J.G., 2005. Adiabatic predictions and observations of cloud droplet spectral broadness. *Atmos. Res.* 73, 203–223.
- Zhang, Q., Quan, J., Tie, X., Huang, M., Ma, X., 2011. Impact of aerosol particles on cloud formation: Aircraft measurements in China. *Atmos. Environ.* 45, 665–672.
- Zhao, C., et al., 2006. Aircraft measurements of cloud droplet spectral dispersion and implications for indirect aerosol radiative forcing. *Geophys. Res. Lett.* 33.
- Zhao, C., et al., 2012. Aerosol first indirect effects on non-precipitating low-level liquid cloud properties as simulated by CAM5 at ARM sites. *Geophys. Res. Lett.* 39.
- Zhao, C., Zhao, L., Dong, X., 2019. A case study of stratus cloud properties using in situ aircraft observations over Huanghua, China. *Atmosphere* 10, 19.
- Zhao, C., et al., 2020. Aerosol characteristics and impacts on weather and climate over the Tibetan Plateau. *Natl. Sci. Rev.* 7, 492–495.